Cell Reports, Volume *9*

Supplemental Information

The RNA-Editing Enzyme ADAR1 Controls Innate Immune Responses to RNA

Niamh M. Mannion, Sam M. Greenwood, Robert Young, Sarah Cox, James Brindle, David Read, Christoffer Nellåker, Cornelia Vesely, Chris P. Ponting, Paul J. McLaughlin, Michael F. Jantsch, Julia Dorin, Ian R. Adams, A.D.J. Scadden, Marie Öhman, Liam P. Keegan, and Mary A. O'Connell

Experimental Procedures

Editing assays

Editing assays were performed as described previously (Rice et al. 2012). RNA editing was identified as an A-to-G change within the cDNA sequence, and the editing percentage was calculated by (G / (A + G)) × 100. Results are the average of at least three separate experiments and are expressed relative to wildtype editing levels, which were normalized to be 100%. Statistical significance was determined by ANOVA with Dunnett's post-hoc tests, or by two-tailed t tests, as appropriate.

RNA extraction and gene expression analysis by qRT-PCR

Total RNA was extracted with Trizol reagent (Invitrogen) and treated with TURBO DNase (Ambion, Life Technologies). The isolated RNA was reverse transcribed with Superscript II (Invitrogen) with oligo-dT or random hexamers according to the manufacturers' instructions. Quantitative PCR was subsequently performed with gene-specific primers (Table S4) and SYBR Green I Master reagent (Roche) using the Lightcycler 480 system (Roche). Analysis of target gene expression was calculated by relative quantification ($2^{-\Delta\Delta Ct}$) as described (Livak and Schmittgen, 2001), with all genes being normalized to the housekeeping genes. Statistical significance was determined by One-way Analysis of Variance (ANOVA) with Bonferroni's or Dunnett's post-hoc tests, or by unpaired two-tailed Student's t-tests, as appropriate.

Fluc mRNA and short dsRNA oligonucleotide transfections

Short dsRNAs were designed from Dharmacon and capped *Fluc* mRNA was *in vitro* transcribed from pLuc-MCS as described (Wormington et al., 1996). *Adar1*$^{-/-}$*; p53*$^{-/-}$ PiggyBac MEFs were transfected in six-well plates at a confluency of 2 x 10^5 with Lipofectamine-2000 (LF-2000; Invitrogen). Typically, cells were transfected with 120 pmol dsRNA (80 pmol specific and 40 pmol control) and 500 ng *Fluc* mRNA (400 ng *Fluc* and 100 ng Rluc). Mock transfections were performed with LF-2000 alone. Cells were harvested 6, 12 or 24 hr post-transfection.

Mouse Embryonic Fibroblast cultures

At E10.5 whole embryos were minced and cultured in high-glucose DMEM with 10% FCS, 1% sodium pyruvate, 1% NEAAs and 1% penicillin/streptomycin, initially in a 6-well plate (Cellstar) and then transferred into 25cm^2 flasks. For nutrient starvation, culture medium was replaced with DMEM and 1% penicillin/streptomycin for either 72 or 144 hours.

Staged mouse embryo collection.

Embryos were taken at defined time points (E10.5, E11.5 etc.) with noon on the morning that a plug was detected being defined as E0.5. The embryos were dissected out of the uteri and yolk sacs and were imaged on a Leica stereo microscope with an exposure time of 0.05s and automatic color balancing. Staging was confirmed using morphological features.

Mouse Histology, Haemotoxylin and Eosin staining

Sections were cleared in xylene then rehydrated in serial dilutions of alcohol. The samples were stained with Mayers haematoxylin for 4 minutes and aqueous eosin for 2 minutes, dehydrated in alcohol and xylene and mounted in DPX. Sections were viewed with color brightfield imaging (Zeiss Axioplan II) and an exposure time of 0.05s.

Mouse genotyping

The tails tips were removed and treated with DNAreleasy (Anachem) according to manufacturer's instructions. Genotypes were verified by PCR with Platinum Taq (Invitrogen). Primers used for genotyping of *Adar1*$^{-/-}$ and *Ifnar1*$^{-/-}$ genotypes were as in previous publications (Hartner et al., 2004; Yoshida et al., 2005). Primers used for genotyping of *Mavs*$^{-/-}$ were as follows:

Mavs^{+} sense, 5'-CAAGTGGGAATCCAGTGAATCAG-3';

Mavs^{+} antisense, 5'-AGGAGAGCCAAGAATGGGAAGC-3;

Mavs^{-} sense, 5'-TTAGGATTGGCTCGGCAGTTAG-3';

Mavs^{-} antisense, 5'-TTCAGATGTAGAAGGCGATGGG-3'.

Mouse transcriptome analyses

RNA-Seq reads were mapped to the mm9 assembly with TMAP (available from http://ioncommunity.lifetechnologies.com/docs/DOC-2101), with reads that mapped to multiple locations randomly assigned a best-scoring location. All other parameters were left at their default. Transcripts were assembled separately for each tissue sample and genotype with Cufflinks, and differential expression between these was assessed by Cuffdiff (Machnicka et al., 2013). Transcripts which contained repetitive elements were identified by intersecting them with RepeatMasker annotations (Smit, AFA, Hubley, R & Green, P. RepeatMasker Open-3.0. 1996-2010 http://www.repeatmasker.org).

To identify changes in expression at specific repetitive element loci in the polyA+ RNA Seq data, paired RNA sequencing reads were mapped to the mm9 assembly of the mouse genome and the UCSC

'known gene' model with TopHat (http://tophat.cbcb.umd.edu/) under stringent conditions allowing no mismatches, insertions or deletions. Reads mapping to unique sites in the genome were recovered by filtering the resulting alignments, and intersected with Repeatmasker annotations of the mouse genome (http://genome.ucsc.edu/). Loci associated with more than 1 read for every million mapped reads in the library were considered further. For these loci, differences in read abundance between datasets were identified with EdgeR (http://www.ncbi.nlm.nih.gov/pmc/articles/PMC2796818/) in R (http://www.r-project.org/).

An additional set of co-ordinates corresponding to LTR-flanked endogenous retroviruses was generated from the UCSC Repeatmasker annotations of the mm9 assembly of the mouse genome in a manner similar to that previously described (Karimi et al., 2011). Briefly, LTR loci belonging to the same repetitive element that were separated by less than 9kb and in the same orientation were assembled into pairs. LTR pairs were annotated based on any internal LTR retrotransposon sequence present between the LTRs, and LTR pairs flanking only sequences belonging to the same LTR retrotransposon were selected. Mapped reads overlapping these LTR-flanked endogenous retrovirus co-ordinates were identified and analyzed as described for the Repeatmasker annotations.

Molecular modeling of dsRNA and RIG-I structures.

Images and superpositions were made with UCSF-Chimera (Pettersen et al., 2004). See Protein Data Base (PDB), for references to structures.

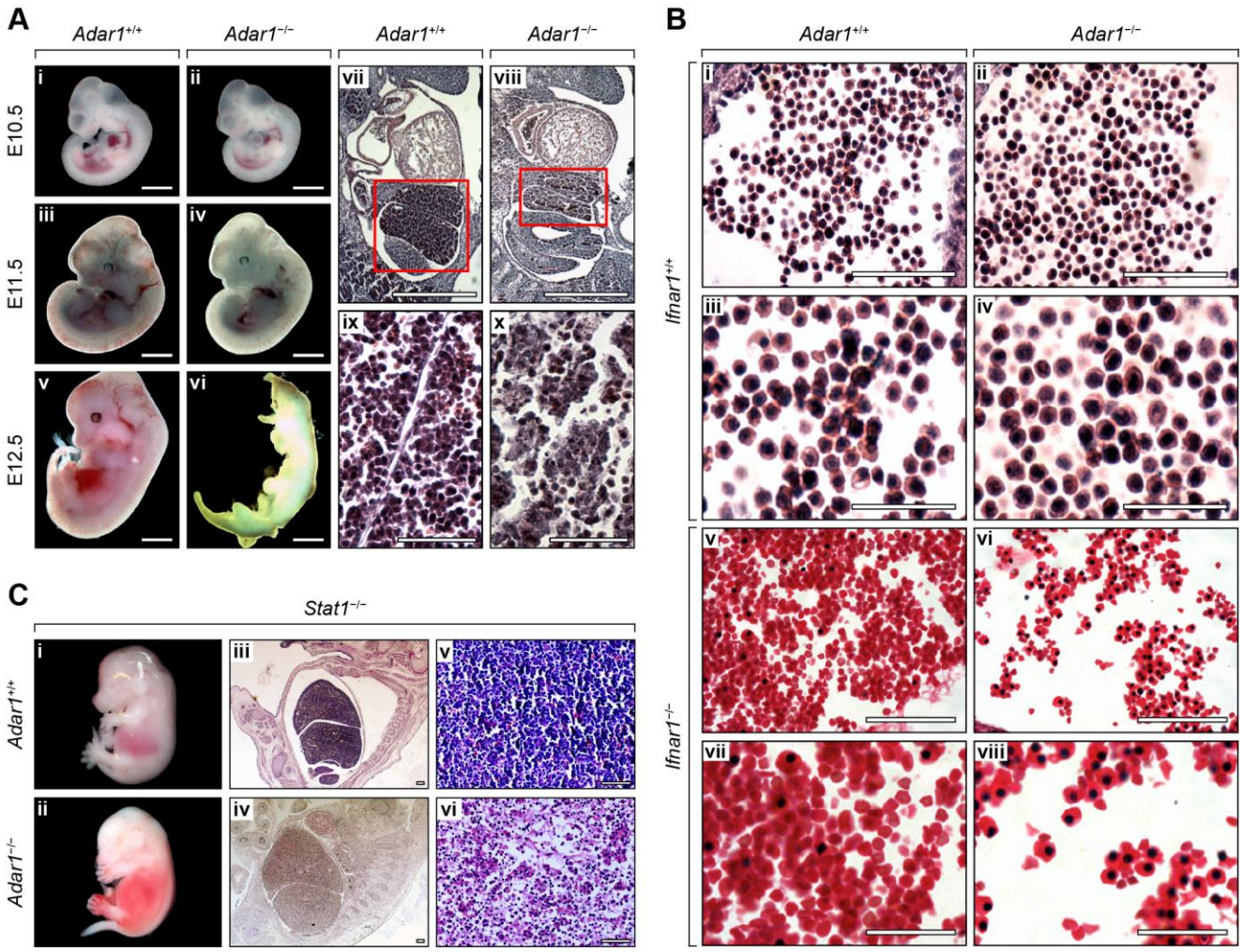

Figure S1, Related to Figure 1. Viability, liver integrity, and peripheral blood in *Adar1* mutant fetal mice.

(**A**) Viability and liver integrity in *Adar1* mutant fetal mice. (i-vi) Whole embryos of wildtype (i, iii, v) and *Adar1* mutant (ii, iv, vi) progeny at E10.5 (i, ii), E11.5 (iii, iv) and E12.5 (v, vi). (vii-x) Whole embryo (vii, viii) and corresponding liver sections (ix, x) of wildtype (vii, ix) and *Adar1* mutant (viii, x) progeny at E11.5. Fetal livers outlined by red boxes. Scale bars: i-viii, 1 mm; ix and x, 50 µm. (**B**) Peripheral blood in *Adar1*; *Ifnar1* mutant fetal mice. (i-iv) Erythrocytes of wildtype (i, iii) and *Adar1* mutant (ii, iv) progeny at E11.5. (v-viii) Erythrocytes of *Ifnar1* (v, vii) and *Adar1*; *Ifnar1* (vi, viii) mutant progeny at E15.5. Scale bars: i, ii, v, vi, 50 µm; iii, iv, vii, viii, 25 µm. (**C**) Viability and liver integrity in *Adar1*; *Stat1* mutant fetal mice. Whole embryos (i, ii) and corresponding liver sections (iii-vi) of *Stat1* (i, iii, v) and *Adar1*; *Stat1* (ii, iv, vi) mutant progeny at E14.5. Scale bars: 100 µm.

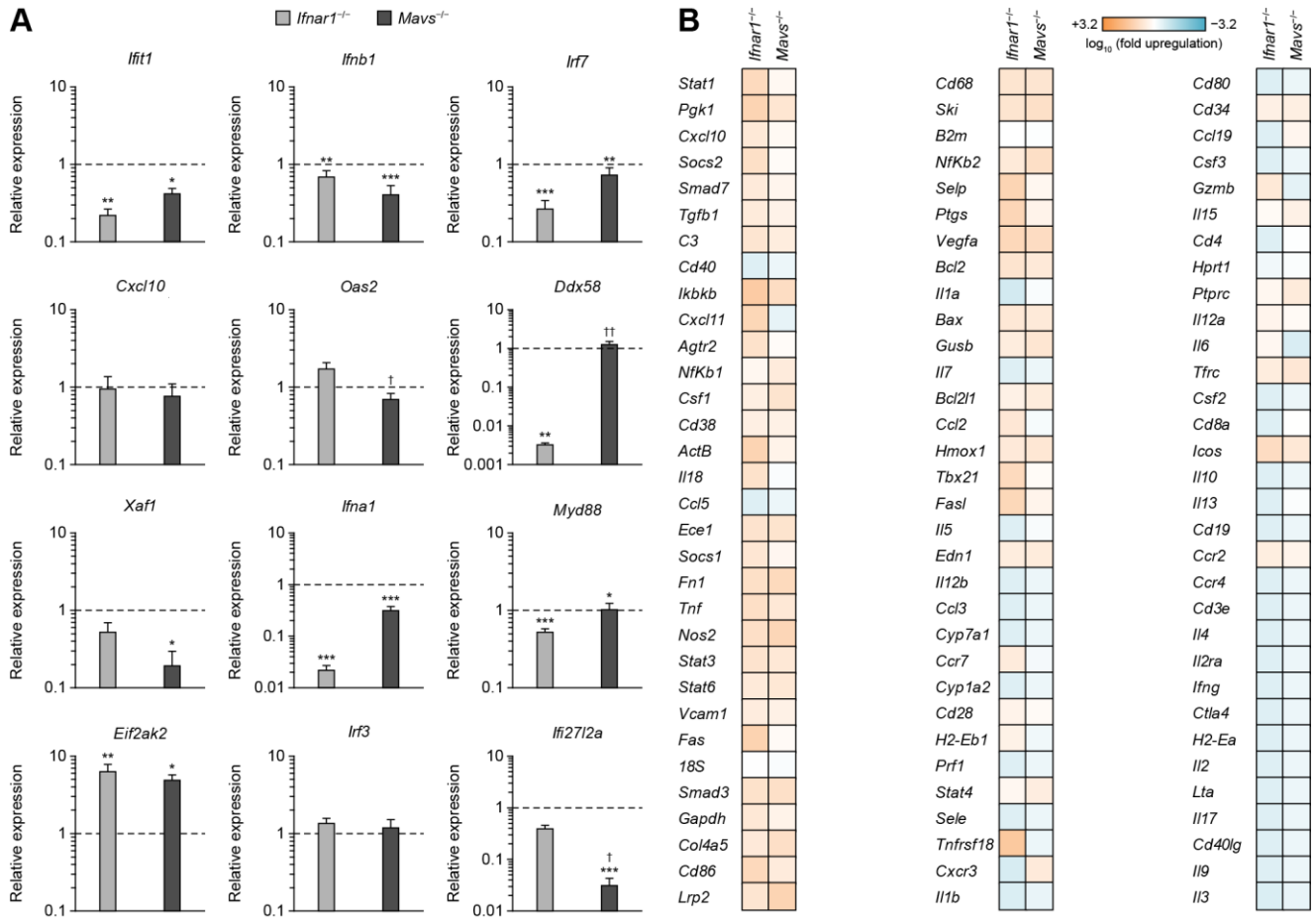

Figure S 2, Related to Figure 3. Pro-inflammatory cytokine expression in *Ifnar1* and *Mavs* mutant embryos.

(**A**) Expression levels for an array of twelve ISGs measured in *Ifnar1* and *Mavs* mutant E11.5 whole embryos. For each gene, values are expressed relative to wildtype (WT) levels, which are all 1 (dashed lines). Error bars, s.e.m. * $p<0.05$; ** $p<0.01$; *** $p<0.001$ versus WT; † $p<0.05$; †† $p<0.01$ versus *Ifnar1*$^{-/-}$. (**B**) Heat map showing expression levels for an array of 96 pro-inflammatory cytokines measured *Ifnar1* and *Mavs* mutant E11.5 whole embryos. For each gene, values are expressed relative to WT levels, which are all 0 following $\log_{10}$-transformation and hence are not shown (white in color).

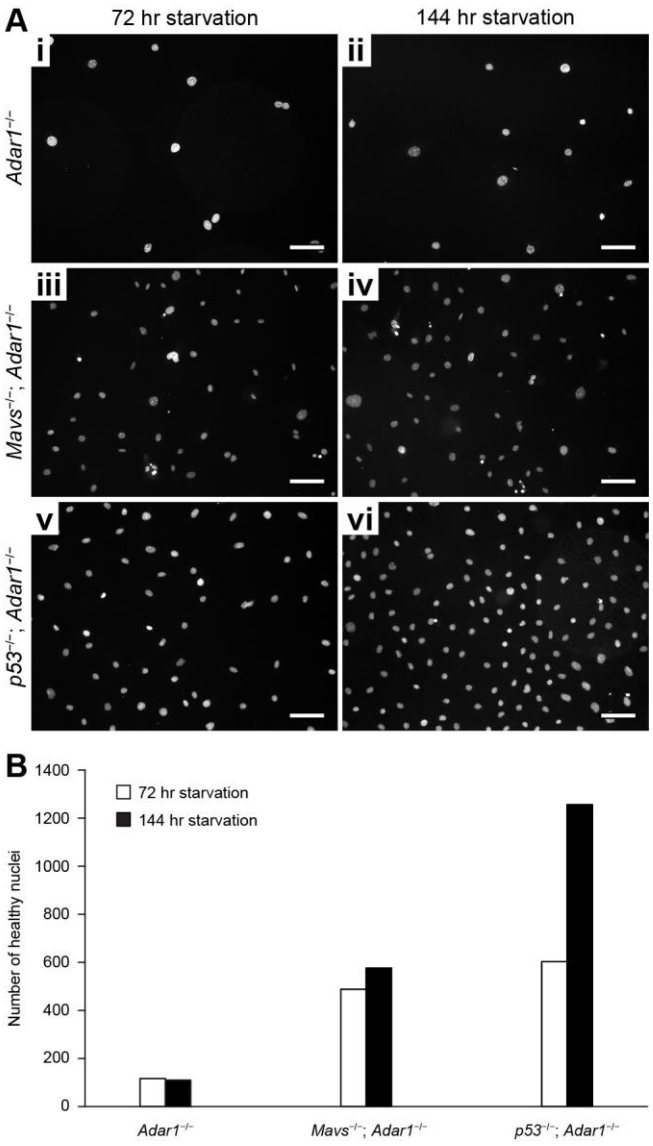

Figure S3, Related to Figure 5. Survival of cultured *Adar1* mutant mouse embryonic fibroblasts (MEFs) following nutrient starvation.

(**A**) DAPI staining of *Adar1* (i, ii), *Adar1*; *Mavs* (iii, iv) and *Adar1*; *p53* (v, vi) mutant MEFS following nutrient starvation for 72 (i, iii, v) or 144 hours (ii, iv, vi). Scale bars: 100 µm. (**B**) Quantification of survival of *Adar1*, *Adar1*; *Mavs* and *Adar1*; *p53* mutant MEFS following nutrient starvation for 72 or 144 hours.

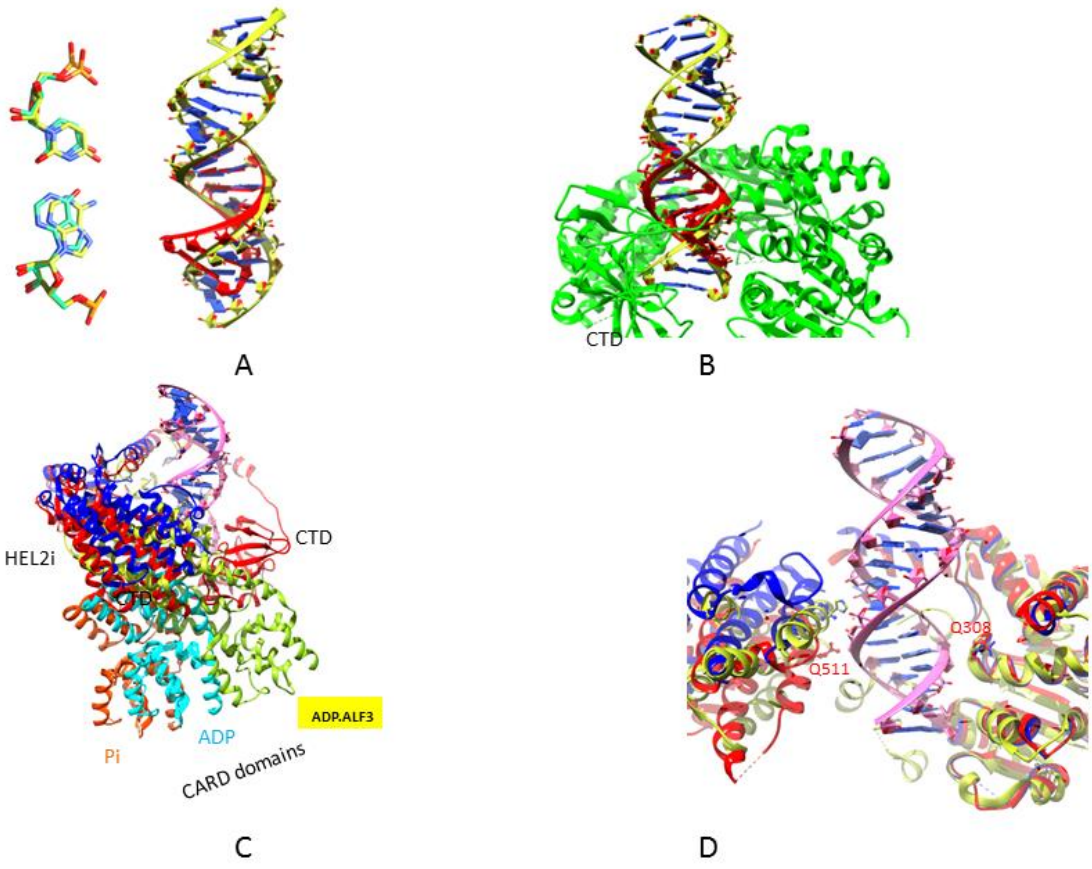

Figure S4 Related to Figure 5. Alterations in dsRNA structure due to I-U wobble base pairs and predicted effects on RLR interactions with edited dsRNA.

(A) Comparison of A-U base pair (carbons yellow) with I-U base pair (carbons green) shows that inosine or uracil form the wobble base pair when one of the bases moves inwards, leaving an indent in the surface of the minor groove. I-U wobble base pairs also distort the path of IU dsRNA (red) compared to canonical ds RNA (yellow). A structure of a tandem two IU-containing dsRNA (pdb code 409D) was superposed on dsRNA (yellow) from the RIG-I ADP-AlF_3 complex (code 4a36). Bases upstream of I-U wobble base pairs were used to make the dsRNA superposition in order to show how distortion due to two IU bases redirects the RNA backbone. (B) Superposition of the two IU dsRNA structure on the bound dsRNA in a structure of dsRNA-bound, nucleotide-free RIG-I. The distortion of the dsRNA path by the two I-U base pairs directs the RNA (red) away from the path of canonical RNA (yellow) so that contacts with the CTD are not made in the same way and the RNA may pass over the CTD and out of the complex. When more than two tandem I-U base pairs are present all such structural effects are expected to be more severe. The image shows two IU dsRNA (code 409D; red) superposed on dsRNA in the structure of nucleotide free RIG-I-dsRNA complex (code 2zda;green). (C) The HEL2i domains of RIG-I transition from one base to the next along the minor groove of regular dsRNA during the nucleotide hydrolysis cycle. The image shows superposed conformations that capture the structure and domain movements of RIG-I at sequential steps in the ATP binding, hydrolysis and release cycle (Kowalinski et al., 2011; Luo et al., 2011). Conformations are: with phosphate (red; code 2ykg); with ADP (blue; code 3zd7) and with ADP-AlF_3 (yellow; 4a36). All structures were superposed through fitting their dsRNA onto the dsRNA (pink) in the ADP-AlF_3 structure. Release of 2CARD domains for signaling may not be due primarily to structural clashes with other domains during the hydrolysis cycle. Pendant 2CARD domains modeled back onto the HEL2i domain at steps in the ATP hydrolysis cycle

do not clash dramatically with the CTD. To predict the position of the 2CARD domain at each step in the cycle 2CARD domains were modeled onto each state of RIG-I using the HEL2i contacts observed in the 2CARD domain-containing RNA-free RIG-I structure (code 4a2w) via superposition of HEL2i domains. Corresponding 2CARD domains are shown in different hues of the color of the state to which they have been modeled. (D) The HEL2i domain moves in one base steps around the minor groove and along one strand of regular dsRNA in the different conformations (same colors as in C). Protein structure behind the plane of the RNA has been removed to give a clearer view of the RNA contacts. Note that Q511 in HEL2i and the alpha helices in the lower part of HEL2i are in different positions as the nucleotide hydrolysis cycle progresses (the residue equivalent to Q511 is a histidine in the duck RIG-I:RNA:ADP.AlF_3 structure, code 4A36, yellow). On the other hand Q381 in HEL1and its following loop do not change positions substantially even though the superposition is made using only the dsRNA; movements of HEL1 and HEL2 domains along the dsRNA major groove are not captured in this series of dsRNA blunt end-associated RIG-I complexes. Release of 2CARD from Hel2i may be responsive to perturbations in Hel2i-RNA interaction caused by I-U base pairs or other irregularities in the dsRNA.

Table S1, Related to Figure 1. Survival of mouse embryos with different *Adar1* genotypes in the C57Bl6N/129 mixed genetic background and from crosses of *Adar1*$^{+/-}$, *Adar1*$^{+/-}$; *Stat1*$^{-/-}$ or *Adar1*$^{+/-}$; *Ifnar1*$^{+/-}$ C57Bl6N/129 parents.

Parents	Day	Litters	Embryos	*Adar1*$^{+/+}$	*Adar1*$^{+/-}$	*Adar1*$^{-/-}$		Exp. −/−
Adar1$^{+/-}$ × *Adar1*$^{+/-}$	E 10.5	3	22	4	14	4		5.50
	E 11.5	2	22	10	10	2		5.50
	E 12.5	4	17	6	9	2		4.25
	E 13.5	2	12	5	7	0		3.00
	E 14.5	2	15	6	9	0		3.75
	E 15.5	1	5	2	3	0		1.25
	Total		93	33	52	8		
Adar1$^{+/-}$; *Stat1*$^{-/-}$ × *Adar1*$^{+/-}$; *Stat1*$^{-/-}$	E12.5	1	11	1	8	2		2.75
	E14.5	2	12	4	5	3		3.00
	E15.5	4	8	5	3	0		2.00
	E17.5	1	4	1	3	0		1.00
	Total		35	11	19	5		
Adar1$^{+/-}$; *Ifnar1*$^{+/-}$ × *Adar1*$^{+/-}$; *Ifnar1*$^{+/-}$				*Adar1*$^{+/+}$	*Adar1*$^{+/-}$	*Adar1*$^{-/-}$	Total	Exp.
			Ifnar1$^{+/+}$	15	30	0	45	48.75
			Ifnar1$^{+/-}$	34	59	0	93	97.50
			Ifnar1$^{-/-}$	12	45	0	57	48.75
			Total	61	134	0	195	
			Exp.	48.75	97.50	48.75		

Table S2, Related to Figure 2. Biological Process GO Term and transcripts significantly upregulated in *Adar1* E11.5 embryos relative to *Adar1; Mavs* and wildtype embryos.

GOTERM_BP_FAT	Count	%	p-value	Benjamini
Immune response	19	5.0	4.90E-18	1.00E-15
Response to virus	10	2.6	1.50E-13	1.60E-11
Innate immune response	6	1.6	6.40E-06	4.50E-04
Defense response	8	2.1	1.00E-04	5.30E-03
Negative regulation of viral reproduction	2	0.5	5.00E-03	1.90E-01
Cytokine-mediated signaling pathway	3	0.8	8.60E-03	2.60E-01
ISG15-protein conjugation	2	0.5	1.00E-02	2.60E-01
Regulation of interferon-alpha production	2	0.5	1.70E-02	3.70E-01
Regulation of viral reproduction	2	0.5	2.00E-02	3.80E-01
Response to exogenous dsRNA	2	0.5	3.00E-02	4.70E-01
Regulation of interferon-beta production	2	0.5	3.40E-02	4.90E-01
Regulation of type I interferon production	2	0.5	3.70E-02	4.80E-01
Response to dsRNA	2	0.5	5.40E-02	5.90E-01

Gene Name	Locus Name (Cufflinks)	*Adar1; Mavs*	*Adar1*	$\log_2$(Fold Change)	p-value	q-value (Benjamini-Hochberg)
Apol9b	XLOC_094945	0.00	1.26	1.80E+308	7.52E-06	6.47E-03
Gm4951	XLOC_128259	0.00	2.13	1.80E+308	8.42E-05	4.89E-02
Ifit3	XLOC_138638	0.05	22.21	8.90E+00	0.00E+00	0.00E+00
I830012O16Rik	XLOC_138639	0.02	6.15	8.22E+00	6.87E-06	6.07E-03
Mx1	XLOC_106134	0.08	23.03	8.21E+00	0.00E+00	0.00E+00
Oas1g	XLOC_203165	0.04	11.79	8.18E+00	7.73E-14	1.95E-10
Oas1b	XLOC_202010	0.11	27.85	7.99E+00	0.00E+00	0.00E+00
Mx2	XLOC_105462	0.14	29.98	7.75E+00	2.29E-13	5.63E-10
Isg15	XLOC_187036	0.36	63.07	7.43E+00	0.00E+00	0.00E+00
Gbp3	XLOC_168972	0.08	10.29	7.09E+00	1.41E-07	1.78E-04
Oas1a	XLOC_203166	0.28	34.31	6.95E+00	0.00E+00	0.00E+00
Irgm1	XLOC_038421	0.36	41.76	6.85E+00	0.00E+00	0.00E+00
Rsad2	XLOC_053856	0.13	14.71	6.79E+00	4.22E-15	1.22E-11
Rtp4	XLOC_105122	0.18	18.56	6.67E+00	0.00E+00	0.00E+00
Usp18	XLOC_220522	0.96	93.07	6.61E+00	0.00E+00	0.00E+00
Oasl2	XLOC_201950	0.24	22.78	6.55E+00	0.00E+00	0.00E+00
Nlrc5	XLOC_254311	0.03	2.63	6.38E+00	1.67E-10	3.05E-07
Sp100	XLOC_000666	0.08	4.59	5.90E+00	1.61E-07	2.00E-04
Gbp2	XLOC_168974	0.11	6.34	5.81E+00	9.55E-13	2.23E-09
Bst2	XLOC_254937	6.16	306.37	5.64E+00	0.00E+00	0.00E+00
Gbp7	XLOC_168971	0.09	4.39	5.62E+00	0.00E+00	0.00E+00
Oasl1	XLOC_201951	0.30	14.06	5.57E+00	3.49E-10	6.01E-07
Irgm2	XLOC_036933	0.23	10.73	5.56E+00	3.42E-14	8.95E-11
Rnf213	XLOC_037880	1.91	85.12	5.47E+00	5.00E-12	1.02E-08
Parp14	XLOC_105743	0.16	6.59	5.39E+00	4.27E-12	9.11E-09
Zbp1	XLOC_150091	0.06	2.43	5.36E+00	1.71E-05	1.28E-02
Ifih1	XLOC_148677	0.24	9.42	5.32E+00	6.74E-11	1.27E-07
Tnfsf10	XLOC_167987	0.02	0.53	5.10E+00	2.54E-06	2.55E-03
Ifitm3	XLOC_239976	3.90	131.04	5.07E+00	0.00E+00	0.00E+00
Stat1	XLOC_000439	2.47	80.27	5.02E+00	2.22E-14	6.06E-11
Igtp	XLOC_036932	1.23	38.42	4.96E+00	0.00E+00	0.00E+00
D14Ertd668e	XLOC_082583	0.04	1.27	4.85E+00	1.55E-06	1.64E-03
Parp12	XLOC_220956	1.33	37.89	4.84E+00	0.00E+00	0.00E+00
Ddx58	XLOC_185588	2.17	61.25	4.82E+00	0.00E+00	0.00E+00
Iigp1	XLOC_128262	0.27	7.46	4.81E+00	6.37E-11	1.23E-07
Samd9l	XLOC_220800	0.09	2.42	4.70E+00	0.00E+00	0.00E+00
Lgals3bp	XLOC_039548	0.40	9.34	4.54E+00	1.73E-06	1.77E-03
Slfn8	XLOC_038999	0.03	0.59	4.35E+00	1.98E-06	2.01E-03
F830016B08Rik	XLOC_128261	0.02	0.43	4.18E+00	7.09E-06	6.16E-03
Hspa1a	XLOC_117289	0.24	4.10	4.12E+00	3.11E-15	9.25E-12
Slfn5	XLOC_037338	0.20	3.14	3.99E+00	6.14E-05	3.79E-02
Trim21	XLOC_239557	1.67	24.03	3.85E+00	0.00E+00	0.00E+00
Xaf1	XLOC_037145	1.07	14.66	3.78E+00	1.51E-14	4.24E-11
Hspa1b	XLOC_117288	0.68	8.80	3.68E+00	0.00E+00	0.00E+00
Gbp5	XLOC_168970	0.06	0.75	3.68E+00	3.29E-07	3.94E-04
Ifi27l1	XLOC_053617	0.99	12.12	3.61E+00	7.56E-08	1.03E-04
Tap1	XLOC_116463	1.01	11.79	3.54E+00	3.46E-14	8.95E-11
Tor3a	XLOC_002252	1.91	21.08	3.47E+00	1.54E-12	3.36E-09
BC006779	XLOC_150243	0.90	9.58	3.41E+00	1.77E-11	3.49E-08
Tlr3	XLOC_254757	0.09	0.87	3.31E+00	5.37E-09	7.98E-06
Nmi	XLOC_148617	1.26	12.02	3.26E+00	2.38E-09	3.65E-06
Cmpk2	XLOC_053236	2.49	22.79	3.19E+00	5.20E-06	4.86E-03
Socs1	XLOC_105523	0.79	6.70	3.09E+00	1.16E-08	1.63E-05
Oas1c	XLOC_203163	0.34	2.88	3.08E+00	6.00E-05	3.73E-02
Lgals9	XLOC_038958	0.38	2.61	2.77E+00	1.27E-05	9.75E-03
Slfn2	XLOC_037340	0.56	3.78	2.75E+00	1.88E-09	2.98E-06
Psmb8	XLOC_116464	0.74	4.26	2.52E+00	7.24E-05	4.28E-02
Trim30a	XLOC_239633	1.49	8.50	2.51E+00	1.60E-06	1.66E-03
Zc3hav1	XLOC_220951	3.08	14.74	2.26E+00	7.99E-08	1.06E-04
Ifit2	XLOC_138637	0.86	3.53	2.04E+00	7.86E-07	8.77E-04
A230004M16Rik	XLOC_036556	2.38	8.10	1.77E+00	2.31E-05	1.66E-02

Table S3, Related to Figure 4. RLTR10C-flanked MMERVK10C and IAPLTR1-flanked IAPEz transposable elements changing in *Adar1*; *Mavs* E15.5 liver versus *Mavs*. Co-ordinates are for NCBI37/mm9 assembly. Total number of mapped reads: *Mavs*, 54,000,000; *Adar1*; *Mavs*, 64,000,000.

TE	Chr	Start	End	Strand	$\log_2$ FC	$\log_2$ CPM	Counts (*Mavs*)	Counts (*Adar1*;*Mavs*)	qRT-PCR primer sets
RLTR10C-MMERVK10C	5	15,187,632	15,194,869	−	8.0175	−0.8423	0	59	iv
	5	15,054,856	15,062,032	−	5.7100	0.1488	2	116	iii, vii, xi
	13	23,352,381	23,359,527	+	2.7190	0.7107	23	153	vi
	13	58,241,432	58,248,529	−	3.2099	−0.5327	7	79	ii, viii
	14	56,415,873	56,423,313	+	2.0484	−0.1239	19	79	
	5	100,415,544	100,422,649	−	1.6765	−0.5751	17	55	
	13	24,860,274	24,863,990	−	1.4096	3.8102	414	1100	
	3	96,117,385	96,124,499	−	1.1613	3.2446	316	707	
	12	8,627,820	8,634,932	−	0.8309	-0.1430	35	62	
	13	93,386,879	93,395,379	−	0.2049	1.7780	172	198	
	8	3,945,963	3,952,931	−	0.1621	1.8987	190	213	
	18	54,029,084	54,036,235	−	0.0236	0.6322	83	84	
	18	6,796,375	6,803,515	−	−0.2883	0.7505	100	82	
	8	34,480,312	34,485,057	+	−0.3431	2.0943	258	209	
	4	109,368,480	109,373,507	−	−0.4193	1.8825	228	170	
	3	96,312,129	96,319,233	−	−6.3183	1.9785	442	5	i, v
IAPLTR1-IAPEz	6	28,874,174	28,879,353	−	5.5295	-0.8807	1	57	
	4	126,685,763	126,692,935	+	2.2903	0.1473	20	99	
	4	147,207,610	147,214,767	−	0.7340	0.0222	41	68	
	13	112,484,442	112,491,030	−	0.4150	0.2519	55	73	
	18	21,420,271	21,427,386	+	0.2248	0.4926	70	82	
	7	86,481,951	86,487,482	−	0.2195	2.4415	271	316	
	11	105,889,559	105,894,874	−	0.1357	2.1286	225	247	
	4	41,401,767	41,407,033	+	0.1240	1.7011	168	183	
	12	74,411,979	74,416,847	−	0.1022	6.8835	6150	6602	
	1	129,788,561	129,793,831	−	−0.0080	0.0484	56	56	
	8	74,752,127	74,756,849	−	−0.1072	0.0986	60	56	
	8	23,661,639	23,668,765	+	−0.1291	0.0879	60	55	
	2	84,345,366	84,350,578	+	−0.1817	0.9637	112	99	
	12	32,712,887	32,717,249	+	−0.3026	0.7584	101	82	
	16	32,148,162	32,153,425	+	−0.5155	0.6369	99	69	
	11	116,250,718	116,256,023	+	−0.8876	0.9523	136	73	
	2	154,179,998	154,185,328	+	−1.4739	−0.4422	59	21	
	6	31,749,369	31,754,637	−	−1.6161	0.1500	91	30	

Table S4, related to Figures 3, 4, 5. Primers used for qRT-PCR.

Name		Sequence 5' to 3'	Description	Accession Number
Actb-Oligo(dT)	F	ACATTGGCATGGCTTTGTTT	Beta actin gene; 3' UTR	GenBank NM_007393.3
	R	GTTTGCTCCAACCAACTGCT		
Cxcl10-Oligo(dT)	F	TCCTTGTCCTCCCTAGCTCA	Chemokine (C-X-C motif) ligand 10 gene; 3' UTR	GenBank NM_021274.1
	R	ATAACCCCTTGGGAAGATGG		
Ddx58-Oligo(dT)	F	ACTCCCCTTCCAGGACATTT	DEAD (Asp-Glu-Ala-Asp) box polypeptide 58 gene; 3' UTR	GenBank NM_172689.3
	R	ACTGTTGACCTCCAGGGTTG		
Eif2ak2-Oligo(dT)	F	TGCCGTGGTTTTCCTTTAAC	Eukaryotic translation initiation factor 2-alpha kinase 2 gene; 3' UTR	GenBank NM_011163.4
	R	CAGGCCCAGCAATTAACAAT		
Ifi27l2a-Oligo(dT)	F	TCAGCTCAACTCAAAGCCTGT	Interferon alpha-inducible protein 27 like 2A gene; 3' UTR	GenBank NM_029803.2
	R	TTTTAGGAACACCAGCCCATA		
Ifit1-Oligo(dT)	F	CCCTGTCTAGCAGGCAATTC	Interferon-induced protein with tetratricopeptide repeats 1 gene; 3' UTR	GenBank NM_008331.3
	R	GGACATTAGCAAAGGGTGGA		
Ifit1-RP	F	AGAGAGTCAAGGCAGGTTTCTG	Interferon-induced protein with tetratricopeptide repeats 1 gene; exonic	GenBank NM_008331.3
	R	ATTCTCTCCCATGGTTGCTG		
Ifit3-RP	F	TTTCCCATCAGCACAGAAAC	Interferon-induced protein with tetratricopeptide repeats 3 gene; exonic	GenBank NM_010501.2
	R	TTCAGCTGTGGAAGGATCG		
Ifna1-Oligo(dT)	F	CTGCTGGCTGTGAGGAAATA	Interferon alpha gene; 3' UTR	GenBank NM_010502.2
	R	CACATTGGCAGAGGAAGACA		
Ifnb1-Oligo(dT)	F	GCCTCAGAATGAGTGGTGGT	Interferon beta gene; 3' UTR	GenBank NM_010510.1
	R	TCTGTTTTCCTTTGACCTTTCA		
Irf3-Oligo(dT)	F	CAAGGCTCAGTCTTCCCATC	Interferon regulatory factor 3 gene; 3' UTR	GenBank NM_016849.4
	R	CGTAGGGACAATGTGTGTGC		
Irf7-Oligo(dT)	F	TCTCGGCTTGTGCTTGTCTA	Interferon regulatory factor 7 gene; 3' UTR	GenBank NM_016850.3
	R	TTGGGAGTTGGGATTCTGAG		
Isg15-RP	F	TAATTCCAGGGGACCTAGAGC	ISG15 ubiquitin-like modifier gene; exonic	GenBank NM_015783.3
	R	ACACCAGGAAATCGTTACCC		
Myd88-Oligo(dT)	F	ACTGGCCTGAGCAACTAGGA	Myeloid differentiation primary response gene (88); 3' UTR	GenBank NM_010851.2
	R	TGTCCCAAAGGAAACACACA		
Mx1-RP	F	TGGAAGCACTGTCTGGAGTC	Myxovirus (influenza virus) resistance 1 gene; exonic	GenBank NM_010846.1
	R	CTCAATTTCAGCACCAGAGG		
Xaf1-Oligo(dT)	F	GCTGGATTCCGAAGATTGAA	XIAP associated factor 1 gene; 3' UTR	GenBank NM_001037713.3
	R	AGGAAAGGAAGCTGGAAAGC		
Actb-RP (Young et al., 2007)	F	CAGCTTCTTTGCAGCTCCTT	Beta actin gene; exonic	GenBank X03672.1
	R	CACGATGGAGGGGAATACAG		
MMERVK10C-i	F	CCAATCAGGGTATGAGACACG*	RLTR10C long terminal repeat; 5' & 3'	Repbase RLTR10B2
	R	AAAGACCTTTTGCCCAGAGC		
MMERVK10C-ii	F	AACCAATCCGGGTATGAGAC	RLTR10C long terminal repeat; 5' & 3'	Repbase RLTR10B2
	R	GATTGCAGAGGCGAAAAGAC		
MMERVK10C-iii	F	CTGGGCTTGAAGTCTTTTCG	RLTR10C long terminal repeat; 5'	Repbase RLTR10B2
	R	GAAGAATGACGCTGCAACAG		
MMERVK10C-iv	F	ATCTTCAGGCAAGAGCGAAG	Internal region of MMERVK10C; 5' UTR	Repbase MMERVK10C
	R	ACAGTCTGTTTTGCGGGAAC		
MMERVK10C-v	F	GAAGGGCAGCGACTTTGTAG	Internal region of MMERVK10C; gag	Repbase MMERVK10C
	R	GCGCGCATCTTCTTTTTC		
MMERVK10C-vi	F	ACCATGGAAAGGGAAAGGAC	Internal region of MMERVK10C; gag	Repbase MMERVK10C
	R	CCCTGCATTTGAAAGAGGTC		
MMERVK10C-vii	F	TCAGCAGGATTGGACATCTG	Internal region of MMERVK10C; gag/pro	Repbase MMERVK10C
	R	AGGCCCACTTTATCCTTTGG		
MMERVK10C-viii	F	TGCTTCTGGGCCTGTTAATC	Internal region of MMERVK10C; pro	Repbase MMERVK10C
	R	AAAAGCCCTGTCCTTCCTTC		
MMERVK10C-ix (Reichmann et al., 2012)	F	CTTACCCTGCAAAAGGTGGA	Internal region of MMERVK10C; env	Repbase MMERVK10C
	R	TGGATGCCACACAACTCATT		
MMERVK10C-x (Reichmann et al., 2012))	F	CCATATGCTGTGGACTGGTG	Internal region of MMERVK10C; env	Repbase MMERVK10C
	R	GCCGTTTTCAATGGCTAAAA		
MMERVK10C-xi (Reichmann et al., 2012)	F	CCAATCAGGGTATGAGACACG*	RLTR10C long terminal repeat; 3'	Repbase RLTR10B2
	R	AAGAACGACACTGCAACAGG		
Control dsRNA (Vitali and Scadden, 2010)	F	GGUCCGGCUCCCCCAAAUGdTdT	Short double stranded RNA oligonucelotide	-
	R	dTdTCCAGGCCGAGGGGGUUUAC		
IU dsRNA (Vitali and Scadden, 2010Vitali and Scadden, 2010))	F	GGUCCGGCIIUICCAAAUGdTdT	Short double stranded RNA oligonucelotide	-
	R	dTdTCCAGGCCGUUIUGGUUUAC		

* Identical oligomers

SUPPLEMENTAL REFERENCE

Hartner, J.C., Schmittwolf, C., Kispert, A., Muller, A.M., Higuchi, M., and Seeburg, P.H. (2004). Liver Disintegration in the Mouse Embryo Caused by Deficiency in the RNA-editing Enzyme ADAR1. J Biol Chem *279*, 4894-4902.

Karimi, M.M., Goyal, P., Maksakova, I.A., Bilenky, M., Leung, D., Tang, J.X., Shinkai, Y., Mager, D.L., Jones, S., Hirst, M., *et al.* (2011). DNA methylation and SETDB1/H3K9me3 regulate predominantly distinct sets of genes, retroelements, and chimeric transcripts in mESCs. Cell Stem Cell *8*, 676-687.

Kowalinski, E., Lunardi, T., McCarthy, A.A., Louber, J., Brunel, J., Grigorov, B., Gerlier, D., and Cusack, S. (2011). Structural basis for the activation of innate immune pattern-recognition receptor RIG-I by viral RNA. Cell *147*, 423-435.

Livak, K.J., and Schmittgen, T.D. (2001). Analysis of relative gene expression data using real-time quantitative PCR and the 2(-Delta Delta C(T)) Method. Methods *25*, 402-408.
Luo, D., Ding, S.C., Vela, A., Kohlway, A., Lindenbach, B.D., and Pyle, A.M. (2011). Structural insights into RNA recognition by RIG-I. Cell *147*, 409-422.

Machnicka, M.A., Milanowska, K., Osman Oglou, O., Purta, E., Kurkowska, M., Olchowik, A., Januszewski, W., Kalinowski, S., Dunin-Horkawicz, S., Rother, K.M., *et al.* (2013). MODOMICS: a database of RNA modification pathways--2013 update. Nucleic Acids Res *41*, D262-267.

Pettersen, E.F., Goddard, T.D., Huang, C.C., Couch, G.S., Greenblatt, D.M., Meng, E.C., and Ferrin, T.E. (2004). UCSF Chimera--a visualization system for exploratory research and analysis. J Comput Chem *25*, 1605-1612.

Reichmann, J., Crichton, J.H., Madej, M.J., Taggart, M., Gautier, P., Garcia-Perez, J.L., Meehan, R.R., and Adams, I.R. (2012). Microarray analysis of LTR retrotransposon silencing identifies Hdac1 as a regulator of retrotransposon expression in mouse embryonic stem cells. PLoS Comput Biol *8*, e1002486.

Vitali, P., and Scadden, A.D. (2010). Double-stranded RNAs containing multiple IU pairs are sufficient to suppress interferon induction and apoptosis. Nat Struct Mol Biol *17*, 1043-1050.
Wormington, M., Searfoss, A.M., and Hurney, C.A. (1996). Overexpression of poly(A) binding protein prevents maturation-specific deadenylation and translational inactivation in Xenopus oocytes. EMBO J *15*, 900-909.

Yoshida, H., Okabe, Y., Kawane, K., Fukuyama, H., and Nagata, S. (2005). Lethal anemia caused by interferon-beta produced in mouse embryos carrying undigested DNA. Nat Immunol *6*, 49-56.

Young, D.W., Hassan, M.Q., Pratap, J., Galindo, M., Zaidi, S.K., Lee, S.H., Yang, X., Xie, R., Javed, A., Underwood, J.M., *et al.* (2007). Mitotic occupancy and lineage-specific transcriptional control of rRNA genes by Runx2. Nature *445*, 442-446.